

# Flavonoids from *Polypodium hastatum* as neuroprotective agents attenuate cerebral ischemia/reperfusion injury *in vitro* and *in vivo* via activating Nrf2

Huankai Yao<sup>a</sup>, Ruiqing Wu<sup>a</sup>, Dan Du<sup>a</sup>, Fengwei Ai<sup>a</sup>, Feng Yang<sup>b</sup>, Yan Li <sup>a</sup> and Suhua Qi<sup>c</sup>

<sup>a</sup>Department of Microbial and Biochemical Pharmacy, School of Pharmacy & Jiangsu Key Laboratory of New Drug Research and Clinical Pharmacy, Xuzhou Medical University, Xuzhou, People's Republic of China; <sup>b</sup>School of Stomatology, Xuzhou Medical University, Xuzhou, People's Republic of China; <sup>c</sup>School of Medical Technology & Xuzhou Key Laboratory of Laboratory Diagnostics, Xuzhou Medical University, Xuzhou, People's Republic of China

## ABSTRACT

**Objectives:** Cerebral ischemic stroke is a leading cause of death worldwide. Though timely reperfusion reduces the infarction size, it exacerbates neuronal apoptosis due to oxidative stress. Nuclear factor erythroid 2-related factor 2 (Nrf2) is a transcription factor regulating the expression of antioxidant enzymes. Activating Nrf2 gives a therapeutic approach to ischemic stroke.

**Methods:** Herein we explored flavonoids identified from *Polypodium hastatum* as Nrf2 activators and their protective effects on PC12 cells injured by oxygen and glucose deprivation/restoration (OGD/R) as well as middle cerebral artery occlusion (MCAO) mice.

**Results:** The results showed among these flavonoids, AAKR significantly improved the survival of PC12 cells induced by OGD/R and activated Nrf2 in a Keap1-dependent manner. Further investigations have disclosed AAKR attenuated oxidative stress, mitochondrial dysfunction and following apoptosis resulting from OGD/R. Meanwhile, activation of Nrf2 by AAKR was involved in the protective effects. Finally, it was found that AAKR could protect MCAO mice brains against ischemia/reperfusion injury via activating Nrf2.

**Discussion:** This investigation could provide lead compounds for the discovery of novel Nrf2 activators targeting ischemia/reperfusion injury.

## KEYWORDS

Flavonoids; *Polypodium hastatum*; ischemia/reperfusion injury; Nrf2; oxidative stress; apoptosis; PC12 cells; MCAO mice



## 1. Introduction

Cerebral stroke is still a global burden due to the high morbidity and mortality, which has been the major cause of disability and death worldwide [1]. There are two major types of cerebral stroke, ischemic stroke and hemorrhagic stroke. The former accounts for more than 80% [2]. Pathogenesis of cerebral ischemic stroke has revealed there is a core of irreversibly injured necrotic tissue, surrounding which there is a potentially salvageable area called penumbra [3]. In that area, the cells are available to ATP and show delayed apoptosis without oxygen and glucose supply [4]. Thus, the cells in the penumbra are determinants of infarction size. Though timely thrombolysis and endovascular thrombectomy could reduce the infarction size resulting from the occlusion of blood flow, the reperfusion also exacerbates the injury in brain tissue due to the oxidative stress following the overproduction of reactive oxygen species (ROS) [5]. Therefore, targeting oxidative stress is one of the promising therapeutic approaches to attenuate cerebral ischemic stroke.

Nuclear factor erythroid 2-related factor 2 (Nrf2) is a transcription factor belonging to the basic leucine transcription factor family, which regulates the transcription of targeting genes encoding antioxidant enzymes through binding to their antioxidant response elements (ARE) in the promoter region [6]. Under basal condition, Nrf2 is sequestered by Kelch-like ECH-associated protein 1 (Keap1) in cytoplasm, which facilitates the degradation of Nrf2 via ubiquitination.

Whereas oxidants or electrophiles can disrupt the Keap1-Nrf2 complex through covalent modification of the key cysteine residues in Keap1, which leads to the liberation of Nrf2 [7]. Then the free Nrf2 will translocate into nuclei and enhance the expression of target genes at transcription level, which results in the up-regulation of antioxidant enzymes such as heme oxygenase-1 (HO-1), NAD(P)H:quinone oxidoreductase 1 (NQO1), superoxide dismutase (SOD), catalase (CAT), glutathione peroxidase (GPx) and so on [8]. Therefore, activating Nrf2 can attenuate oxidative stress and relevant diseases [9]. In the development of cerebral ischemic stroke, oxidative stress plays a pivotal role and activation of Nrf2 gives a potential strategy to ameliorate ischemia/reperfusion injury [10].

Structure analysis of Keap1-Nrf2 complex has revealed two Keap1 monomers form a dimer and interact with the DLG and ETGE motifs in a Nrf2 using their Kelch domains, respectively [11]. Since the affinity of DLG to Kelch domain is much lower than that of ETGE, it is proposed that Nrf2 binds to Keap1 via a 'hinge and latch' model [12]. Therefore, it has been approved that targeting the Nrf2 binding cavity of Kelch domain will give an effective approach to activate Nrf2 [13]. According to the molecular dynamics simulation and mechanics-generalized Born surface area free energy calculation, the Nrf2 binding cavity can be divided into six subpockets (P1–P6) [14]. Small molecules interacting with the key amino acid residues in those subpockets will directly activate Nrf2 via disrupting the Keap1-Nrf2 complex [15].

**CONTACT** Yan Li  liyan@xzhmu.edu.cn  Department of Microbial and Biochemical Pharmacy, School of Pharmacy & Jiangsu Key Laboratory of New Drug Research and Clinical Pharmacy, Xuzhou Medical University, Xuzhou, Jiangsu 221004, People's Republic of China

© 2024 The Author(s). Published by Informa UK Limited, trading as Taylor & Francis Group  
This is an Open Access article distributed under the terms of the Creative Commons Attribution-NonCommercial License (<http://creativecommons.org/licenses/by-nc/4.0/>), which permits unrestricted non-commercial use, distribution, and reproduction in any medium, provided the original work is properly cited. The terms on which this article has been published allow the posting of the Accepted Manuscript in a repository by the author(s) or with their consent.

Phytochemicals are the important pool to discover Nrf2 activators [16]. Many natural compounds showed significant activity to activate Nrf2 such as sulforaphane, curcumin, resveratrol and so on [17]. *Polypodium hastatum* is a medicinal herb distributed in most areas of China, Japan and Korea. In Chinese folklore, this plant is used to treat respiratory and urinary diseases [18]. Previous phytochemical investigations have revealed there are polyphenols including phenolic acids and flavonoids as the major chemical constituents in this plant [18–20]. As a large class of polyphenols, flavonoids showed various bioactivities. To search natural Nrf2 activators targeting ischemia/reperfusion injury, we have revisited the flavonoids in *Polypodium hastatum* using *in vitro* and *in vivo* models and explored the underlying mechanisms.

## 2. Materials and methods

### 2.1. Chemicals and reagents

3-(4,5-dimethyl-2-thiazolyl)-2,5-diphenyl-2-H-tetrazolium bromide (MTT) assay kit, lactate dehydrogenase (LDH) release assay kit, ROS assay kit, malondialdehyde (MDA) assay kit, SOD assay kit, CAT assay kit, GPx assay kit, reduced glutathione (GSH) and oxidized glutathione disulphide (GSSG) assay kit, cysteinyl aspartate specific proteinase-3 (caspase-3) assay kit, mitochondrial permeability transition pore assay kit, nuclear and cytoplasmic protein extraction kit, bicinchoninic acid (BCA) protein assay kit, and enhanced chemiluminescence (ECL) assay kit as well as 4',6-diamidino-2-phenylindole (DAPI) staining solution, 3,3'-diaminobenzidine (DAB) solution, hematoxylin-eosin (HE) staining solution, rabbit IgG, Fluo-3 AM and rhodamine-123 were provided by Beyotime Biotechnology (Shanghai, China). DyLight 594-conjugated secondary antibody and horseradish peroxidase-labeled secondary antibody were obtained from Abcam (Cambridge, UK). Primary antibodies against B-cell lymphoma-2 (Bcl-2), Bcl-2-associated X (Bax), cleaved caspase-3, Nrf2, Keap1, lamin B1 and  $\beta$ -actin were provided by Proteintech (Rosemont, IL). HO-1 and NQO1 enzyme-linked immunosorbent assay (ELISA) kits were obtained from Colorfulgene Biotechnology (Wuhan, China). The ARE-luciferase reporter plasmid (pGL4.37[*luc2P*/ARE/Hygro]), renilla luciferase reporter plasmid (pRL-TK) and dual-luciferase reporter assay system were purchased from Promega (Madison, WI). Lipofectamine 2000, nimodipine (Nim) and the Nrf2 activator, sulforaphane (SFN) were furnished by Thermo Fisher Scientific (Waltham, MA). Tiron (a superoxide anion radical scavenger) was provided by MedChemExpress (Shanghai, China). LCS-1 (a specific SOD1 inhibitor), 3-amino-1,2,4-triazole (3-AT, a specific CAT inhibitor) and JKE-1674 (a specific GPx4 inhibitor) were obtained from Selleck Chemicals (Houston, TX). Negative control siRNA (NC-siRNA) and Nrf2-siRNA were supplied by Santa Cruz Biotechnology (Dallas, TX). Protein A-Agarose was purchased from Santa Cruz Biotechnology (Santa Cruz, CA).

### 2.2. Phytochemical investigation

The whole plant of *Polypodium hastatum* was collected from Xiamen, Fujian Province, China in August 2019 and identified by Dr Yan Li at the Department of Microbial and Biochemical Pharmacy, School of Pharmacy, Xuzhou Medical University. The voucher specimen (No. 201908003) was deposited at the same institution.

The air-dried plant (3.0 kg) was grounded and extracted with ethanol (20.0 L  $\times$  3) under reflux for 4 h each time. After removing the solvent under reduced pressure, the residue (153.0 g) was suspended in water (1.5 L) and partitioned with petroleum ether (1.5 L  $\times$  3), acetyl acetate (1.5 L  $\times$  3) and *n*-butanol (1.5 L  $\times$  3), successively. The acetyl acetate and *n*-butanol extracts were condensed under reduced pressure to give acetyl acetate residue (58.0 g) and *n*-butanol residue (73.0 g), respectively. The acetyl acetate part was subject to column chromatography (i.d. 8.0 cm) on silica gel (200–300 mesh, 700.0 g) eluted with gradient dichloromethane/methanol (100% 5.0 L, 95% 10.0 L, 90% 20.0 L, 80% 15.0 L, 70% 10.0 L, 60% 10.0 L, 50% 5.0 L, 40% 5.0 L, v/v) and gave 12 fractions. Fraction 5 (5.5 g) was further handled on silica gel (200–300 mesh, 55.0 g) column chromatography (i.d. 3.5 cm) eluted with gradient dichloromethane/methanol (95% 1.0 L, 90% 1.5 L, 80% 1.5 L, 70% 1.0 L, v/v) and then crystallized in ethanol to afford **2** (12.0 mg). Fraction 8 (7.5 g) was separated on Toyopearl HW-40C (800.0 g) column chromatography (i.d. 5.0 cm) with isocratic dichloromethane/methanol (66% 4.0 L, v/v) to give **1** (21.0 mg). The *n*-butanol part was separated on AB-8 porous resin (1.0 kg) column chromatography (i.d. 8.0 cm) eluted with ethanol (30% 15.0 L, 60% 15.0 L, 90% 15.0 L, v/v) to give three fractions. Fraction 1 (27.0 g) was separated on Diaion HP-20SS (300.0 g) column chromatography (i.d. 5.0 cm) eluted with gradient methanol/water (10% 2.0 L, 30% 2.0 L, 60% 2.0 L, 90% 2.0 L, v/v) to afford six subfractions. Subfraction 2 (3.5 g) was handled on ODS (50.0 g) column chromatography (i.d. 2.0 cm) eluted with methanol/water (10% 300.0 mL, 30% 200.0 mL, 50% 400.0 mL, 70% 200.0 mL, 90% 200.0 mL, v/v) and then purified on Sephadex LH-20 (60.0 g) column chromatography (i.d. 2.5 cm) to give **3** (16.0 mg) and **5** (31.0 mg), respectively. Subfraction 3 (1.1 g) was further purified on Sephadex LH-20 (60.0 g) column chromatography (i.d. 2.5 cm) with the elution of isocratic methanol to yield **4** (15.0 mg).

### 2.3. Cell culture and treatment

Rat pheochromocytoma (PC12) cells were supplied by Cell Bank of Shanghai Institute of Biological Sciences, Chinese Academy of Sciences (Shanghai, China) and maintained in Dulbecco's modified Eagle medium (DMEM) including 10% FBS, 100 U/mL penicillin, and 100  $\mu$ g/mL streptomycin at 37°C at a humid atmosphere with 5% CO<sub>2</sub> and 95% air. The cells were divided into control group and experimental groups and treated as our previous description [21]. In brief, after removing the normal culture medium, the cells in experimental groups were cultured in glucose-free DMEM with 95% N<sub>2</sub> and 5% CO<sub>2</sub> at 37°C for 4 h, and then incubation in normal medium with 95% air and 5% CO<sub>2</sub> was implemented for 24 h. During the treatment of OGD/R, the cells in experimental groups were also exposed to certain flavonoids, SFN, Nim, tiron, LCS-1, 3-AT or JKE-1674. The cells in control group were maintained at a normoxic atmosphere.

### 2.4. MTT assay

To evaluate the protective effects of these compounds, MTT assay was performed. Briefly, the cells were treated as above and then 10  $\mu$ L MTT solution was added. After incubation for 4 h at 37°C, 100  $\mu$ L DMSO was added to dissolve the formazan. After another incubation for 4 h at 37°C, the absorbance was read on a microplate reader (BioTek, Winooski, VT) at 570 nm.

### 2.5. LDH release

To reveal the release of LDH, the extracellular LDH activity was detected using the commercially available kit. Briefly, the PC12 cells were treated as above and centrifuged at 400g for 5 min. Then the supernatant was collected and mixed with the working solution. After incubation for 30 min, the absorbance was recorded on a microplate reader at 490 nm. The LDH activity was expressed as the relative percentage of absorbance against a control group.

### 2.6. Dual luciferase reporter assay

Dual luciferase reporter assay was implemented herein to reveal the transcription capacity of Nrf2 in PC12 cells. In the light of the manufacturer's instruction, the PC12 cells were co-transfected with ARE luciferase reporter plasmid (pGL4.37[luc2P/ARE/Hygro]) and renilla luciferase reporter plasmid (pRL-TK) using lipofectamine 2000 and incubated at 37°C for 18 h. Then the cells were treated as above and the luciferase activity was determined using the dual luciferase reporter assay system on a Promega GloMax luminometer (Madison, WI). The transcription capacity of Nrf2 was expressed as relative luciferase activity derived through normalizing the firefly luciferase against the renilla luciferase.

### 2.7. Intracellular ROS level

The production of intracellular ROS was determined using the ROS assay kit. The PC12 cells were treated as above and rinsed with serum-free medium. Then the cells were exposed to 2',7'-dichlorofluorescein diacetate (DCFH-DA) solution in the assay kit and incubated in the dark for 30 min at 37°C. After removing the solution and washing with serum-free medium, the fluorescence of DCF was read on a fluorescence microplate reader (Molecular Devices, San Jose, CA) at an excitation wavelength of 485 nm and emission wavelength of 520 nm.

### 2.8. MDA content

Thiobarbituric acid method was employed to demonstrate the MDA content of PC12 cells. In brief, after treatment, the supernatant of PC12 cells was collected and mixed with a working solution in the assay kit. After boiled for 15 min, the mixture was cooled to room temperature followed by centrifugation at 1000g for 10 min. And the absorbance was monitored at 532 nm.

### 2.9. SOD, CAT and GPx activity

The activity of antioxidant enzymes in PC12 cells including SOD, CAT and GPx was measured using the commercially available assay kits according to the supplier's protocols. The treated cells were washed with PBS and lysed on ice-cold lysis solution. Then the lysates were centrifuged at 12,000g for 5 min, and the supernatant was collected for further analysis after determination of proteins concentration using the BCA assay kit. For the SOD activity assay, 20  $\mu$ L supernatant was mixed with 160  $\mu$ L nitro-blue tetrazolium (NBT)/enzyme working solution and 20  $\mu$ L initiating working solution in the assay kit. Then incubation was carried out at 37°C for 30 min, and the absorbance was

recorded on a microplate reader at 560 nm. For the CAT activity assay, 10  $\mu$ L supernatant was mixed with 10  $\mu$ L H<sub>2</sub>O<sub>2</sub> working solution and 30  $\mu$ L assay buffer solution in the assay kit. After incubation at 25°C for 5 min, terminating solution was added and vortex was performed. Then the mixture was diluted using assay buffer solution with the ratio of 1:4 followed by the addition of chromogenic solution in the kit, and the absorbance was determined on a microplate reader at 520 nm after incubation at 25°C for 15 min. For GPx activity assay, 5  $\mu$ L supernatant was mixed with 178  $\mu$ L GPx assay solution, 5  $\mu$ L GSH solution, and 12  $\mu$ L peroxide solution. After incubation at 25°C for 10 min, 6.6  $\mu$ L 5,5'-dithiobis-(2-nitrobenzoic acid) (DTNB) solution in the kit was added followed by another incubation at 25°C for 10 min. Then the absorbance was read on a microplate reader at 412 nm.

### 2.10. GSH and GSSG levels

To further reveal the GPx activity in PC12 cells, intracellular GSH and GSSG were detected using a commercially available kit herein. Briefly, in light of the supplier's protocol, the cells were treated as above and harvested. After washed with PBS, the cells were treated with protein scavenger M in the kit under freeze-thaw conditions. After centrifugation at 10,000g for 10 min at 4°C, the supernatant was collected as the sample for total GSH analysis. The sample was exposed to 5,5'-dithiobis-2-nitrobenzoic acid (DTNB) and glutathione reductase at 25°C for 5 min. Then NADPH was added and incubation was implemented for 25 min. The absorbance was recorded on a microplate reader at 412 nm. After removing GSH using the scavenger in the assay kit, the GSSG was in the sample detected as above. The GSH/GSSG ratio was calculated according to the supplier's instructions.

### 2.11. Intracellular calcium level

To reveal the intracellular calcium level in PC12 cells, the fluorescence probe Fluo-3 AM was employed. In brief, the treated PC12 cells were exposed to Fluo-3 AM at 37°C in the dark for 1 h. Then the cells were washed with PBS three times to clear the extracellular dye. The fluorescence intensity of Fluo-3 was detected on a fluorescence microplate reader at the excitation/emission wavelength of 488/525 nm.

### 2.12. Mitochondrial membrane potential

The mitochondrial membrane potential in PC12 cells was determined using rhodamine-123. The PC12 cells were treated as above and washed with PBS. Then rhodamine-123 was loaded in the dark at 37°C for 20 min. After washing with PBS, the fluorescence intensity was read on a microplate reader at the excitation wavelength of 507 nm and emission wavelength of 525 nm.

### 2.13. Mitochondrial permeability transition pore opening

The mitochondrial permeability transition pore was explored using the assay kit according to the supplier's protocol. The treated PC12 cells were collected and suspended in an assay buffer containing calcium ion. Calcein AM staining solution together with fluorescence quenching solution

including  $\text{CoCl}_2$  was added. After incubation in the dark at 37°C for 30 min, the cells were washed with assay solution to remove the excessive reagents. The fluorescence intensity of calcein was detected on a fluorescence microplate reader at 494/517 nm as excitation/emission wavelength.

#### 2.14. Caspase-3 activity

Colorimetric method was used to determine the activity of caspase-3 in PC12 cells using the commercially available assay kit. Briefly, the PC12 cells were treated as above and then centrifuged at 600g and 4°C for 5 min. After washed with PBS, the cells were lysed on ice with lysis solution in the kit for 15 min. Then the lysates were centrifuged at 20,000g and 4°C for 10 min, and the supernatant was mixed with specific substrate (Ac-DEVD-pNA). After incubation at 37°C for 2 h, the absorbance was recorded on a microplate reader at 405 nm.

#### 2.15. Western blot analysis

The proteins including Bcl-2 and Bax together with nuclear and total Nrf2 in PC12 cells were analyzed by western blot. After being treated as above, the proteins were extracted as per our previous description (Yao et al. 2020) and analyzed by BCA analysis. Then the proteins were separated on 10% sodium dodecyl sulfate polyacrylamide gel electrophoresis (SDS-PAGE) and transferred to polyvinylidene fluoride (PVDF) membranes. After blocking with defatted milk, the blots were incubated with the primary antibodies against Bcl-2 (1:1000), Bax (1:5000), Nrf2 (1:1000),  $\beta$ -actin (1:1000) and lamin B1 (1:10000) at 4°C overnight. After washed with buffer solution including 0.1% Tween-20, the blots were incubated with horseradish peroxidase-labeled secondary antibody at room temperature for 1 h. ECL substrate was used to visualize the blots. Densitometric analysis was carried out using Image J software (NIH, Bethesda, MD).

#### 2.16. Enzyme-linked immunosorbent assay (ELISA)

To reveal the levels of intracellular HO-1 and NQO1 in PC12 cells, ELISA was performed using the assay kits. After quantification using the BCA assay kit, the samples were treated according to the suppliers' protocols. The absorbance was recorded on a microplate reader at 450 nm.

#### 2.17. Immunofluorescence staining

To detect the localization of intracellular Nrf2 in PC12 cells, immunofluorescence staining was employed. Briefly, the PC12 cells were cultured in 12-well microplates with a coverslip in each well and treated as above. Then the cells were washed with PBS and fixed using 4% paraformaldehyde at 4°C for 15 min. After permeabilization using PBS containing 0.1% Triton X-100 for 10 min, the cells were blocked with 1% BSA for 30 min. Then the cells were exposed to the primary antibody against Nrf2 (1:200) at 4°C overnight. After washed with PBS, the cells were incubated with DyLight 594-conjugated secondary antibody at 37°C in the dark. Then the cells were washed with PBS again and exposed to DAPI solution in the dark for 2 min. The coverslips were mounted on glass slides and the images were captured under a fluorescence microscope (Olympus, Tokyo, Japan).

#### 2.18. Nrf2 knockdown assay

To demonstrate the role of Nrf2 activation in the protective effects, siRNA interference assay was performed. The PC12 cells were transfected with NC-siRNA or Nrf2-siRNA according to the producer's protocol. Then western blot analysis was implemented to determine the transfection was attained successfully. Then the transfected PC12 cells were treated as above and subsequently MTT assay was employed to explore the cell viability.

#### 2.19. Co-immunoprecipitation assay

To explore the interaction between Keap1 and Nrf2 in PC12 cells, co-immunoprecipitation assay was carried out. According to the supplier's protocol, the treated cells were harvested and lysed on ice using the RIPA buffer solution. After centrifugation at 10,000g for 10 min at 4°C, the supernatant was collected and pre-clear reaction was implemented using the rabbit IgG together with suspended Protein A-Agarose to remove the non-specific combination. Then the supernatant was incubated at 4°C for 30 min and centrifuged at 1000g for 5 min. The supernatant was collected and incubated with the primary antibody against Nrf2 or rabbit IgG at 4°C for 1 h. Then Protein A-Agarose was added and shook at 4°C overnight. After centrifugation at 1000g for 5 min, the supernatant was carefully aspirated and discarded. Then the pellets were washed with RIPA buffer four times and suspended in an SDS loading buffer. After boiled for 3 min, the samples were analyzed by western blot analysis with respective antibodies.

#### 2.20. Molecular docking

To visualize the binding mode of Keap1 with the flavonoids, the interaction between Keap1 and compound 5 was explored by molecular docking performed by SYBYL X2.1. The 3D structure of compound 5 was established from SYBYL sketch and optimized using Tripos force field and Gasteiger-Huckel charges. The 3D structure of Keap1 Kelch domain was obtained from RSCB Protein Data Bank (PDB code: 4IQK). After extracting the ligand and removing the water molecules, hydrogen atoms and charges were added to the structure of Keap1 Kelch domain. Then the protomol file was generated to produce docking envelope and Surflex-Dock program with default parameters was run for docking calculation.

#### 2.21. Animal model

20 male C57BL/6 mice (8–10 weeks, 20–25 g) were provided by Laboratory Animal Center of Xuzhou Medical University. The mice were randomly divided into four groups including sham group, MCAO group, MCAO + AAKR group (AAKR, 50.0 mg/kg), MCAO + AAKR + ML385 group (AAKR, 50.0 mg/kg; ML385, 30.0 mg/kg). All the mice were housed under the circumstance with 12-h light/dark cycle, approximately 60% relative humidity, and  $25 \pm 2^\circ\text{C}$  temperature. And the mice were freely access to food and water. Focal cerebral ischemia was performed using middle cerebral artery occlusion (MCAO). In brief, mice were anesthetized with 4% isoflurane and maintained at 2% via inhalation. After the left external carotid artery

was completely exposed and ligated, a nylon monofilament was inserted into the internal carotid artery to occlude the middle cerebral artery. After 1 h of occlusion, the monofilament was carefully dismantled to restore the blood flow for 24 h. Mice were eliminated from the groups if they died following ischemia or the cerebral blood flow did not decrease at least 70%. Before 1 h of MCAO, AAKR or ML385 was administered by intraperitoneal injection. Mice in the sham group were exposed to the same surgical procedure except the insertion of a monofilament. And mice in MCAO group were intraperitoneally injected with a vehicle. After aforementioned treatment, the mice were sacrificed under anesthesia with 4% isoflurane, and brain tissues were obtained. The tissues were homogenized at 4°C. After centrifugation at 12,000g and 4°C for 3 min, the supernatant was collected for further analysis of antioxidant enzymes and western blot as above.

## 2.22. HE staining

After perfused with physiological saline, brain tissues were fixed with 4% paraformaldehyde, embedded in paraffin, and cut into sections (4 μm). Then the sections were deparaffinized, rehydrated and stained with hematoxylin–eosin. The sections were observed under a microscope (Olympus, Tokyo, Japan) to assess histopathological changes in the cortex.

## 2.23. Immunohistochemical (IHC) assays

The brain tissues were treated as above and sections (4 μm) were prepared. Then the sections were deparaffinized, and rehydrated. The sections were incubated in 3% H<sub>2</sub>O<sub>2</sub> for 15 min to block endogenous peroxidase. After rinsing with PBS for three times, the sections were exposed to primary antibody against cleaved caspase-3 (1:500) overnight at 4°C. After washed with PBS for three times, secondary antibody was added and incubation was carried out for 15 min. Then the sections were reacted with DAB solution for 5 min. Subsequently, the sections were washed with water and stained with hematoxylin for 1 min. The sections were observed under a microscope.

## 2.24. Statistical analysis

All experimental data were expressed as mean ± standard deviation. GraphPad Prism 8.0 (San Diego, CA) were employed to perform data analysis. Shapiro–Wilk normality test was carried out to validate the data followed a normal distribution. Then one-way analysis of variance (one-way ANOVA) followed by Tukey test was performed for multiple comparisons and Student's *t*-test was implemented for single comparisons. And *p* < .05 was considered as significant difference in statistics.

## 3. Results

### 3.1. Structure elucidation

The <sup>1</sup>H and <sup>13</sup>C NMR spectra were recorded on a Bruker AVANCE III NMR spectrometer. The structures of these compounds obtained were determined by analysis of their <sup>1</sup>H

and <sup>13</sup>C NMR spectra as well as comparison of these data with literature. Their structures were identified as kaempferol-7-*O*-α-*L*-rhamnopyranoside (KR, **1**) [22], kaempferol-3-*O*-α-*L*-arabinofuranoside (juglanin, **2**) [23], 3-*O*-α-*L*-arabinofuranosyl-kaempferol-7-*O*-α-*L*-rhamnopyranoside (AKR, **3**) [24], kaempferol-3,7-*O*-α-*L*-dirhamnopyranoside (kaempferitrin, **4**) [25], and 3-*O*-β-*D*-apiofuranosyl-(1→2)-α-*L*-arabinofuranosyl-kaempferol-7-*O*-α-*L*-rhamnopyranoside (AAKR, **5**) [26] (Figure 1). The <sup>1</sup>H and <sup>13</sup>C NMR data were assigned as follows:

Kaempferol-7-*O*-α-*L*-rhamnopyranoside (**1**): yellow amorphous powder; <sup>1</sup>H NMR (400 MHz, DMSO-*d*<sub>6</sub>) δ: 8.10 (2H, d, *J* = 9.0 Hz, H-2', 6'), 6.94 (2H, d, *J* = 9.0 Hz, H-3', 5'), 6.83 (1H, d, *J* = 1.9 Hz, H-8), 6.43 (1H, d, *J* = 1.9 Hz, H-6), 5.56 (1H, br s, H-1''), 3.32-3.86 (m, H-2'', 3'', 4'', 5'' overlapped with – OH proton signals), 1.14 (3H, d, *J* = 6.4 Hz, H-6''); <sup>13</sup>C NMR (100 MHz, DMSO-*d*<sub>6</sub>) δ: 176.0 (C-4), 161.4 (C-7), 160.3 (C-5), 159.3 (C-4'), 155.7 (C-9), 147.5 (C-2), 136.0 (C-3), 129.6 (C-2', 6'), 121.5 (C-1'), 115.4 (C-3', 5'), 104.6 (C-10), 98.8 (C-1''), 98.3 (C-6), 94.3 (C-8), 71.6 (C-4''), 70.2 (C-3''), 70.0 (C-2''), 69.8 (C-5''), 17.9 (C-6'').

Juglanin (**2**): yellow amorphous powder; <sup>1</sup>H NMR (400 MHz, DMSO-*d*<sub>6</sub>) δ: 8.03 (2H, d, *J* = 8.9 Hz, H-2', 6'), 6.90 (2H, d, *J* = 8.9 Hz, H-3', 5'), 6.46 (1H, d, *J* = 1.9 Hz, H-8), 6.21 (1H, d, *J* = 1.9 Hz, H-6), 5.63 (1H, d, *J* = 6.4 Hz, H-1''), 4.16 (1H, m, H-2''), 3.74 (1H, m, H-5''b), 3.28-3.54 (m, H-3'', 4'', 5''b overlapped with – OH proton signals); <sup>13</sup>C NMR (100 MHz, DMSO-*d*<sub>6</sub>) δ: 177.6 (C-4), 164.3 (C-7), 161.2 (C-5), 159.9 (C-4'), 156.7 (C-9), 156.3 (C-2), 133.4 (C-3), 130.8 (C-2', 6'), 120.7 (C-1'), 115.4 (C-3', 5'), 103.9 (C-10), 108.0 (C-1''), 98.7 (C-6), 93.7 (C-8), 86.3 (C-4''), 77.1 (C-3''), 82.1 (C-2''), 60.8 (C-5'').

3-*O*-α-*L*-arabinofuranosyl-kaempferol-7-*O*-α-*L*-rhamnopyranoside (**3**): yellow amorphous powder; <sup>1</sup>H NMR (400 MHz, DMSO-*d*<sub>6</sub>) δ: 8.09 (2H, d, *J* = 8.5 Hz, H-2', 6'), 6.91 (2H, d, *J* = 8.5 Hz, H-3', 5'), 6.84 (1H, br s, H-8), 6.46 (1H, br s, H-6), 5.65 (1H, br s, H-1'''), 5.57 (1H, br s, H-1''), 3.32-5.30 (m, H-2'', 3'', 4'', 5'', 2''', 3''', 4''', 5''' overlapped with – OH proton signals), 1.13 (3H, *J* = 5.5 Hz, H-6'''); <sup>13</sup>C NMR (100 MHz, DMSO-*d*<sub>6</sub>) δ: 177.8 (C-4), 161.6 (C-7), 160.8 (C-5), 160.1 (C-4'), 157.2 (C-9), 155.9 (C-2), 133.7 (C-3), 130.8 (C-2', 6'), 120.5 (C-1'), 115.4 (C-3', 5'), 108.1 (C-1''), 105.6 (C-10), 99.3 (C-1'''), 98.3 (C-6), 94.6 (C-8), 86.4 (C-4''), 82.1 (C-2''), 77.1 (C-3''), 71.6 (C-4'''), 70.2 (C-3'''), 70.0 (C-2'''), 69.8 (C-5'''), 60.9 (C-5''), 17.9 (C-6'').

Kaempferitrin (**4**): yellow amorphous powder; <sup>1</sup>H NMR (400 MHz, DMSO-*d*<sub>6</sub>) δ: 7.77 (2H, d, *J* = 7.4 Hz, H-2', 6'), 6.90 (2H, d, *J* = 7.4 Hz, H-3', 5'), 6.77 (1H, s, H-8), 6.44 (1H, s, H-6), 5.53 (1H, s, H-1''), 5.28 (1H, s, H-1'''), 3.00-4.00 (m, H-2'', 3'', 4'', 5'', 2''', 3''', 4''', 5''' overlapped with – OH proton signals), 1.11 (3H, d, *J* = 3.9 Hz, H-6'''); <sup>13</sup>C NMR (100 MHz, DMSO-*d*<sub>6</sub>) δ: 177.9 (C-4), 161.6 (C-7), 160.9 (C-5), 160.1 (C-4'), 157.7 (C-

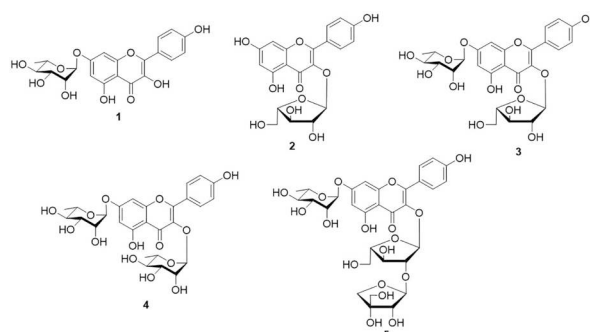
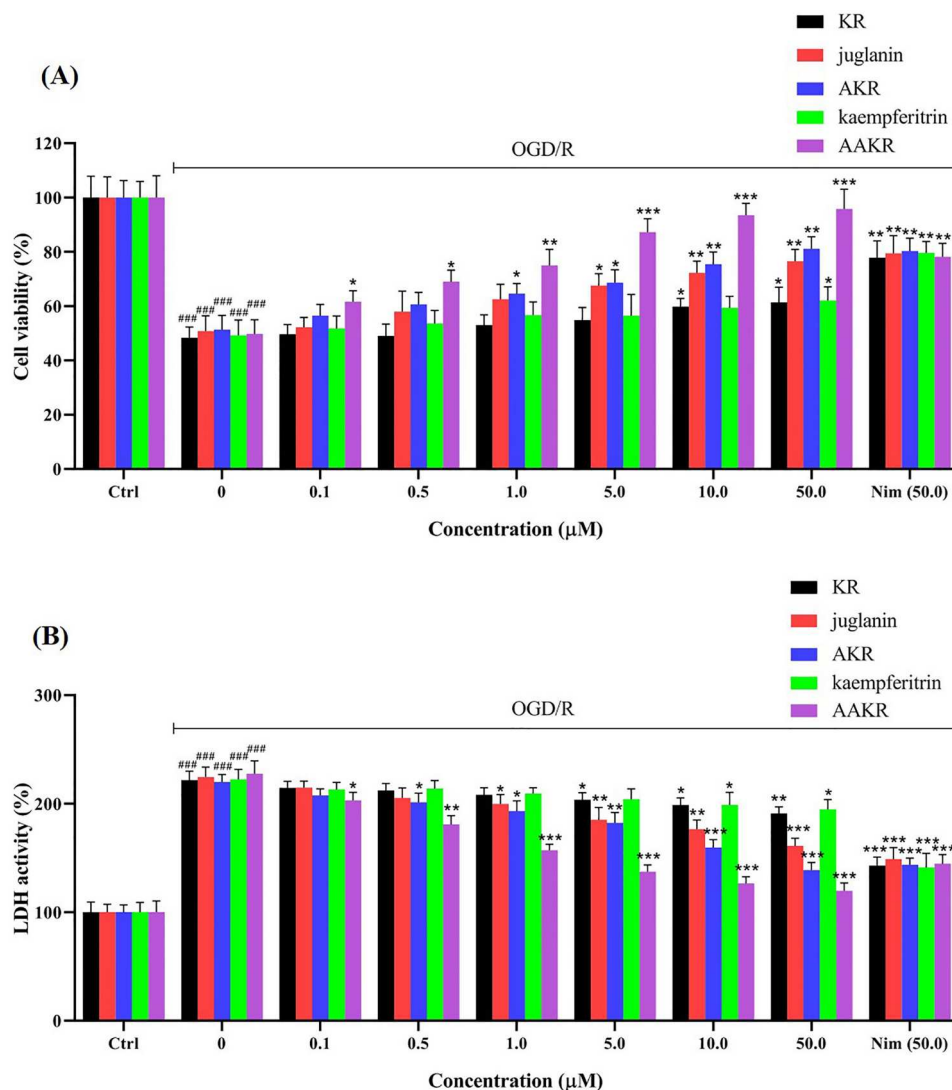


Figure 1. Chemical structures of flavonoids from *Polypodium hastatum*.



**Figure 2.** Effects of the flavonoids on the survival of PC12 cells injured by OGD/R. (A) MTT assay. (B) Extracellular LDH activity. Nimodipine (Nim) was used as a reference drug.  $n = 3$ ,  $###p < .001$  vs control group,  $*p < .05$ ,  $**p < .01$  and  $***p < .001$  vs OGD/R group.

9), 156.1 (C-2), 134.5 (C-3), 130.7 (C-2', 6'), 120.3 (C-1'), 115.4 (C-3', 5'), 105.7 (C-10), 101.8 (C-1''), 99.4 (C-1'''), 98.4 (C-6), 94.5 (C-8), 71.6 (C-4''), 71.1 (C-5''), 70.6 (C-4'''), 70.3 (C-2''), 70.2 (C-2'''), 70.1 (C-3''), 70.0 (C-3'''), 69.8 (C-5'''), 17.9 (C-6''), 17.4 (C-6''').

3-O-β-D-apiofuranosyl-(1→2)-α-L-arabinofuranosyl-kaempferol-7-O-α-L-rhamnopyranoside (**5**): yellowish amorphous powder;  $^1\text{H}$  NMR (400 MHz, DMSO- $d_6$ )  $\delta$ : 8.03 (2H, d,  $J = 8.7$  Hz, H-2', 6'), 6.92 (2H, d,  $J = 8.7$  Hz, H-3', 5'), 6.84 (1H, br s, H-8), 6.46 (1H, br s, H-6), 5.81 (1H, br s, H-1'''), 5.57 (1H, br s, H-1''), 5.08 (1H, d,  $J = 2.8$  Hz, H-1'''), 3.30-5.50 (m, H-2'', 3'', 4'', 5'', 2''', 4''', 5''', 2''', 3''', 4''', 5''') overlapped with -OH proton signals), 1.14 (3H,  $J = 6.0$  Hz, H-6''');  $^{13}\text{C}$  NMR (100 MHz, DMSO- $d_6$ )  $\delta$ : 177.8 (C-4), 161.6 (C-7), 160.8 (C-5), 160.1 (C-4'), 157.2 (C-9), 155.9 (C-2), 133.3 (C-3), 130.8 (C-2', 6'), 120.4 (C-1'), 115.5 (C-3', 5'), 107.8 (C-1''), 106.1 (C-1'''), 105.6 (C-10), 99.4 (C-1'''), 98.4 (C-6), 94.5 (C-8), 87.8 (C-4''), 85.7 (C-2''), 78.7 (C-3'''), 76.1 (C-2'''), 75.6 (C-3'''), 73.5 (C-4'''), 71.6 (C-4'''), 70.2 (C-3'''), 70.1 (C-2'''), 69.8 (C-5'''), 63.0 (C-5'''), 60.3 (C-5''), 17.9 (C-6''').

### 3.2. Flavonoids improve the survival of PC12 cells injured by OGD/R

To evaluate the protective effects of these flavonoids, MTT assay was performed first. The results showed AAKR from

0.1 μM could significantly attenuate the poor cell viability resulting from OGD/R, which even afforded more protective effects than the reference drug nimodipine at 50.0 μM. And juglanin and AKR also afforded moderate protective effects on PC12 cells injured by OGD/R while the effects of KR and kaempferitrin were weak (Figure 2(A)). Meanwhile, extracellular LDH activity in PC12 cells was detected to further validate the protective effects of these flavonoids (Figure 2(B)). As a result, AAKR remarkably reduced the activity of extracellular LDH, which was similar to the effects of nimodipine at 50.0 μM. And these results indicated AAKR could suppress the release of LDH induced by OGD/R. Meanwhile, it was also found juglanin and AKR attenuated the release of LDH moderately, but compounds KR and kaempferitrin displayed poor effects against that. Taken together, these results implied of all the five flavonoids, AAKR possessed significant protective effects against the injury caused by OGD/R, and juglanin and AKR gave moderate effects. Nevertheless, the protection of KR and kaempferitrin was poor.

### 3.3. Flavonoids interact with Keap1 to activate Nrf2

To demonstrate the effects of these flavonoids on the activation of Nrf2, we have assessed the transcription capacity of Nrf2 binding to ARE in PC12 cells using a dual luciferase

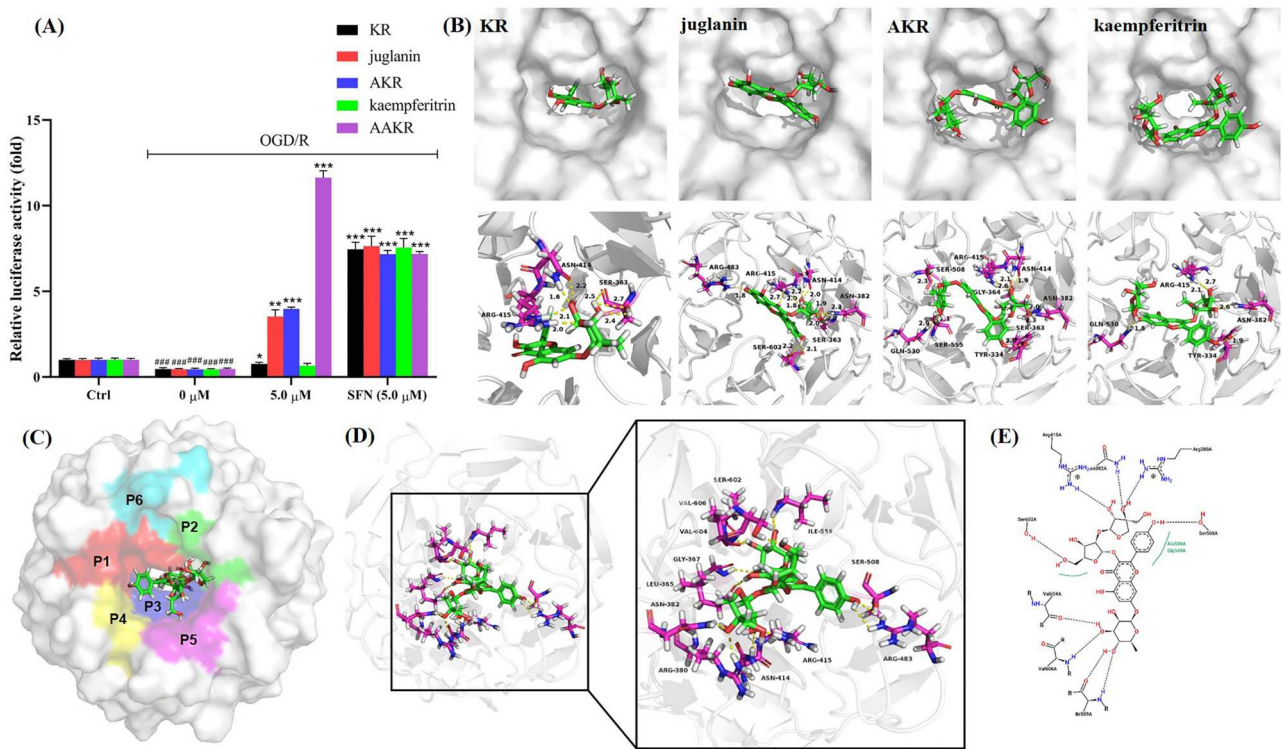


**Figure 3.** Effects of the flavonoids on the Nrf2 activation in PC12 cells injured by OGD/R. (A) ARE luciferase activity. SNF was used as a reference drug. (B) Binding modes of compounds 1–4 with Keap1 including binding poses and interactions via hydrogen bonds. (C) Binding pose of AAKR in the Nrf2 binding cavity. (D) Interaction for AAKR with Kelch domain via hydrogen bonds. (E) 2D diagram for the interaction between AAKR and Keap1.  $n = 3$ , ###  $p < .001$  vs control group, \*  $p < .05$ , \*\*  $p < .01$  and \*\*\*  $p < .001$  vs OGD/R group.

reporter system. As shown in Figure 3(A), in the presence of AAKR at 5.0 μM, the transcription capacity of Nrf2 was remarkably elevated ( $11.64 \pm 0.40$ ) compared with the cells treated

without that compound ( $0.46 \pm 0.06$ ) and even more potent than the sulforaphane ( $7.17 \pm 0.14$ ). Meanwhile, KR, juglanin and AKR also showed significant enhancement for the

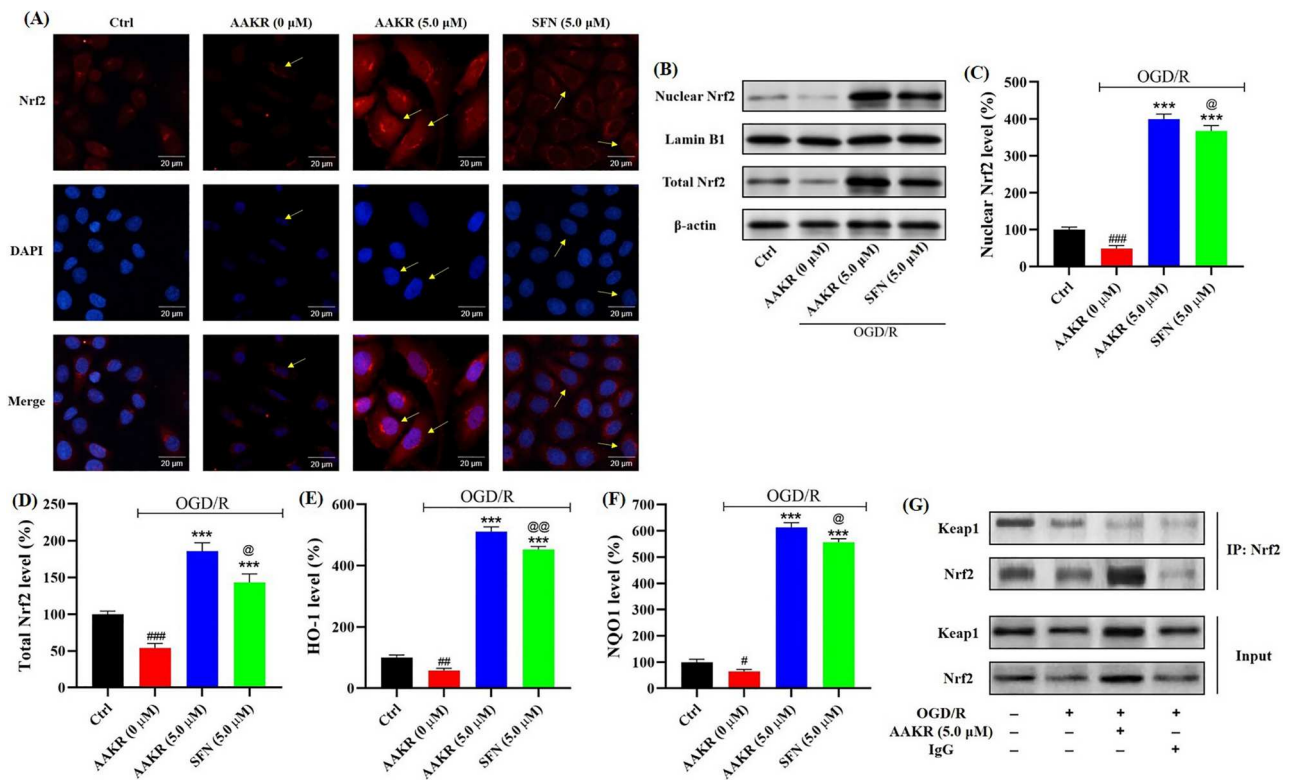


**Figure 4.** Effects of AAKR on Keap1-dependent activation of Nrf2 in PC12 cells injured by OGD/R. (A) Immunofluorescence staining, as the yellow arrows indicated, the red fluorescence represented the intracellular Nrf2, blue fluorescence represented nuclei and the merged purple fluorescence represented the nuclear Nrf2. (B)–(D) Western blot analysis together with densitometric analysis of total and nuclear Nrf2. (E) and (F) HO-1 and NQO1 levels in PC12 cells detected by ELISA. (G) Co-immunoprecipitation assay for Nrf2. IP: Nrf2 was precipitated using its specific antibody. Input: The lysates were analyzed by western blot without precipitation.  $n = 3$ , #  $p < .05$ , ##  $p < .01$  and ###  $p < .001$  vs control group, \*\*\*  $p < .001$  vs OGD/R group, @  $p < .05$  and @@  $p < .01$  vs AAKR group.

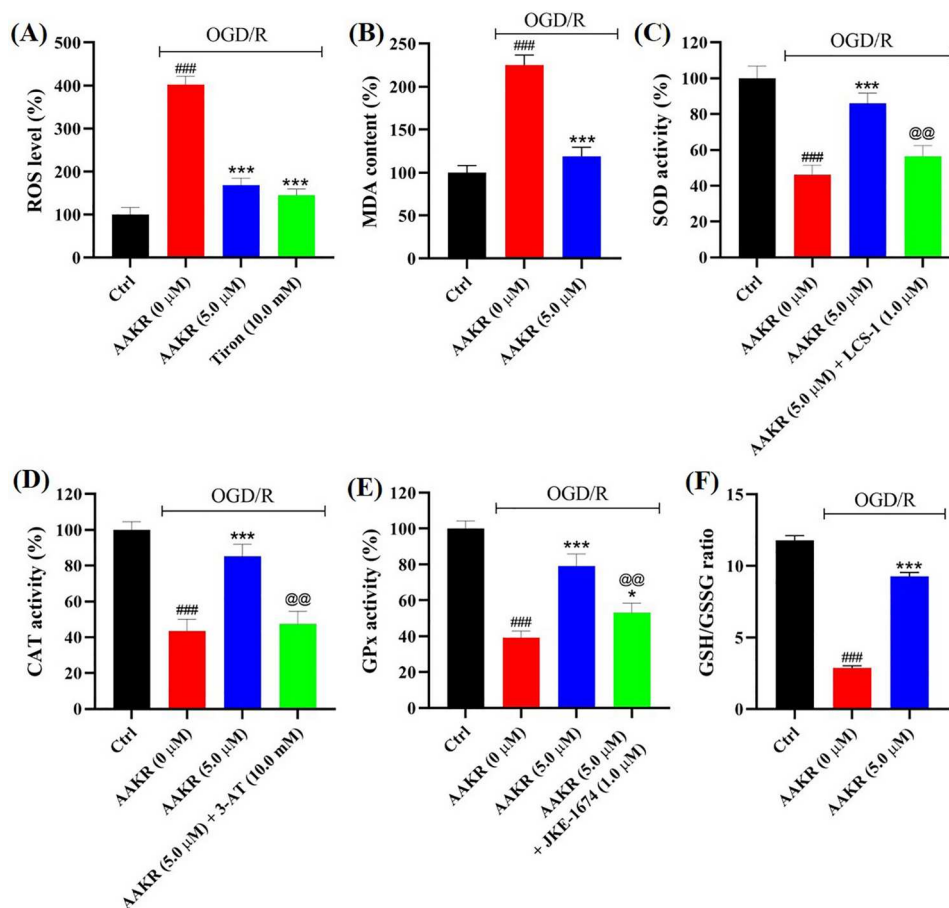


**Figure 5.** Effects of AAKR on oxidative stress induced by OGD/R in PC12 cells. (A) Intracellular ROS levels. (B) MDA content. (C)–(E) SOD, CAT and GPx activity. (F) GSH/GSSG ratio.  $n = 3$ , ### $p < .001$  vs control group, \* $p < .05$  and \*\*\* $p < .001$  vs OGD/R group, @@ $p < .01$  vs AAKR group.

transcription capacity of Nrf2 in PC12 cells. Molecular docking results revealed these compounds could enter the Nrf2 binding cavity and interact with the residues in Kelch domain of Keap1 via hydrogen bonds (Figure 3(B–D)). Of these compounds, AAKR afforded the highest total score as 9.16, which is higher than the *in situ* ligand (total score is 7.66). And other total scores of these compounds are 6.78 for AKR, 6.42 for juglanin, 5.50 for KR and 5.06 for kaempferitrin. In addition to the amino acid residues including Leu365 (2.4 Å), Gly367 (2.4 Å), Ile559 (1.9 and 1.9 Å), Val604 (2.1 Å), and Val606 (2.1 Å), AAKR also interacted with those in the subpockets of Nrf2 binding cavity encompassing Arg415 (1.8 Å), Arg483 (2.3 Å) and Ser508 (2.2 Å) of P1, Arg380 (2.1 Å), Asn382 (2.0 Å) and Asn414 (2.6 Å) of P2, and Ser602 (2.0 Å) of P3 via hydrogen bonds (Figure 3(D)). The 2D diagram gave the indication that there was hydrophobic interaction between the B-ring of AAKR and the residues including Gly509 and Ala556 of P3 (Figure 3(E)). These interactions are the driving forces for AAKR to bind to Keap1 and activate Nrf2. The results indicated that AAKR was the most potent Nrf2 activator of the five flavonoids.

### 3.4. AAKR activates Nrf2 in PC12 cells injured by OGD/R in a Keap1-dependent manner

To demonstrate the effects of AAKR on the activation of Nrf2, immunofluorescence staining was implemented to visualize and locate Nrf2. As a result, AAKR at 5.0 μM increased the level of Nrf2 and promoted its translocation into nucleus from the cytoplasm as the yellow arrows implied in the

immunofluorescence images, which indicated it stabilized and activated Nrf2 (Figure 4(A)). Then western blot analysis together with densitometric analysis has also revealed AAKR resulted in the increment of total and nuclear Nrf2 compared with the group treated without this compound (Figure 4(B–D)). At the same time, as the downstream enzymes the antioxidant enzymes including HO-1 and NQO1 were upregulated by AAKR (511.24 ± 14.83% and 613.57 ± 17.61% for HO-1 and NQO1, respectively) in contrast to the cells injured by OGD/R (58.07 ± 7.07% and 64.82 ± 7.08%, respectively) (Figure 4(E,F)). To elucidate the underlying mechanism of Nrf2 activation by AAKR, co-immunoprecipitation assay was performed. As shown in Figure 4(G), following the precipitation of Nrf2 with itself primary antibody, Keap1 was precipitated in both control group and the group treated without AAKR. Whereas, in the presence of AAKR, the precipitated Keap1 was reduced, which implied this compound could interact with Keap1 to disrupt the formation of Keap1-Nrf2 complex.

### 3.5. AAKR attenuates oxidative stress resulting from OGD/R in PC12 cells

To assess the protective effects of AAKR against oxidative stress, the intracellular ROS was detected herein. The results showed OGD/R gave rise to the overproduction of ROS (402.12 ± 19.68%), which was reversed by AAKR at 5.0 μM (168.47 ± 16.51%). And its effects were similar to Tiron, a superoxide anion radical scavenger (Figure 5(A)). Meanwhile, as the major product of lipid peroxidation, the content of



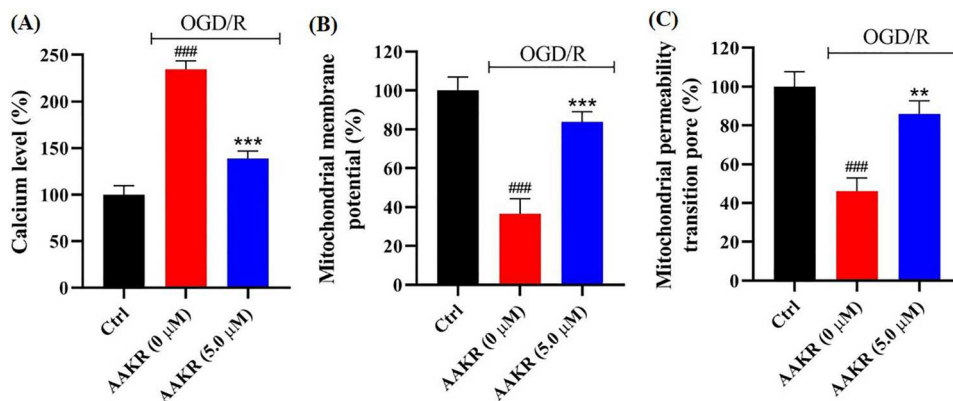


**Figure 6.** Effects of AAKR on mitochondrial dysfunction induced by OGD/R in PC12 cells. (A) Intracellular calcium levels. (B) Mitochondrial membrane potential. (C) Mitochondrial permeability transition pore.  $n = 3$ , ### $p < .001$  vs control group, \*\* $p < .01$  and \*\*\* $p < .001$  vs OGD/R group.

MDA in PC12 cells was measured. It was observed that the excessive generation of MDA resulting from OGD/R was reduced by AAKR ( $118.83 \pm 10.58\%$ ) compared to the group treated without that compound ( $225.05 \pm 11.69\%$ ) (Figure 5(B)). In addition, we have found that OGD/R resulted in the declined activity of SOD ( $46.14 \pm 5.31\%$ ), CAT ( $43.56 \pm 6.57\%$ ) and GPx ( $39.29 \pm 3.61\%$ ) in PC12 cells. Whereas, after exposure to AAKR, the activity of these antioxidant enzymes has been enhanced as  $86.06 \pm 5.74\%$ ,  $85.27 \pm 6.68\%$  and  $79.14 \pm 6.64\%$ , respectively. When the specific inhibitors including LCS-1, 3-AT and JKE-1674 targeting SOD1, CAT and GPx4 were added separately, the enhanced activity for these enzymes by AAKR was reduced (Figure 5(C–E)), which further implied AAKR activated these enzymes to attenuate oxidative stress. Meanwhile, the GSH/GSSG ratio also disclosed AAKR elevated the activity of GPx (Figure 5(F)). Collectively, these results demonstrate AAKR could inhibit oxidative stress induced by OGD/R in PC12 cells.

### 3.6. AAKR ameliorates mitochondrial dysfunction in PC12 cells injured by OGD/R

To disclose the protective effects of AAKR on PC12 cell against the injury resulting from OGD/R, mitochondrial function was evaluated herein. As a result, we have observed OGD/R caused the overload of intracellular calcium ( $234.48 \pm 9.03\%$ ), while in the presence of AAKR

at 5.0 μM, the overloaded calcium was attenuated ( $138.78 \pm 8.08\%$ ) (Figure 6(A)). At the same time, the collapse of mitochondrial membrane potential ( $36.63 \pm 7.66\%$ ) and opening of mitochondrial permeability transition pore ( $46.12 \pm 6.77\%$ ) were also detected in PC12 cells due to OGD/R. However, AAKR significantly reversed the collapse of mitochondrial membrane potential ( $83.89 \pm 5.18\%$ ) as well as mitochondrial permeability transition pore opening ( $85.98 \pm 6.72\%$ ) (Figure 6(B,C)). These observations manifested AAKR ameliorated OGD/R-induced mitochondrial dysfunction in PC12 cells.

### 3.7. AAKR inhibits apoptosis of PC12 cells induced by OGD/R

The proteins related to apoptosis were explored to uncover the protective effects of AAKR. In the present investigation, OGD/R has activated the activity of caspase-3 in PC12 cells ( $264.61 \pm 12.00\%$ ). Whereas, after exposure to AAKR, the activity of caspase-3 was inhibited at  $140.55 \pm 7.56\%$  (Figure 7(A)). Though OGD/R down-regulated the expression of Bcl-2 and up-regulated Bax in PC12 cells, western blot analysis has shown that Bcl-2 was elevated by AAKR while Bax was diminished (Figure 7(B)). Meanwhile, the relative ratio of Bcl-2/Bax further substantiated AAKR inhibited the apoptosis induced by OGD/R in PC12 cells (Figure 7(C)).

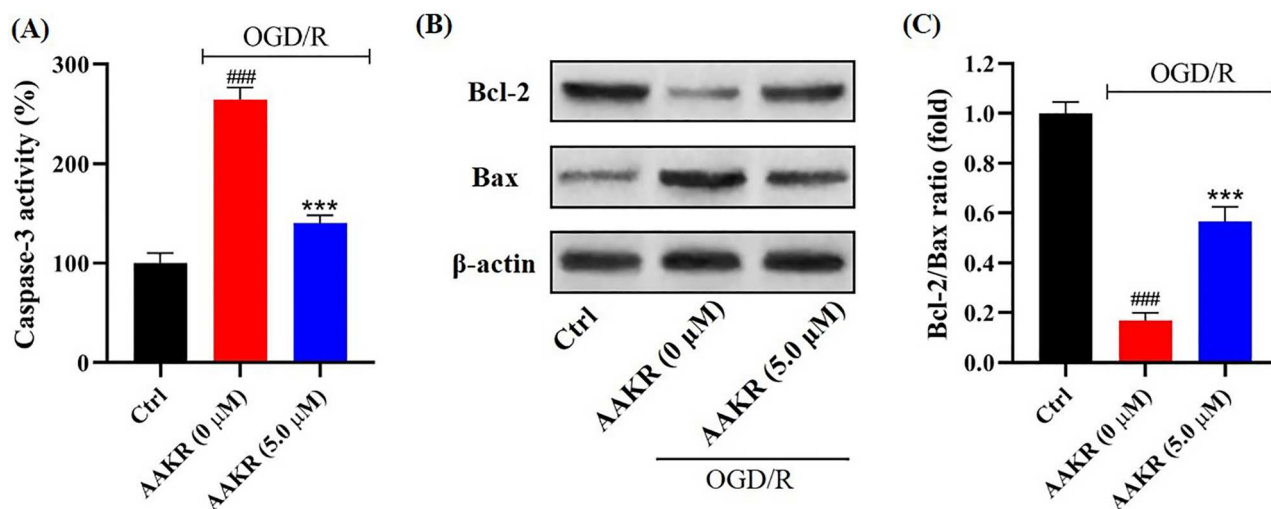


**Figure 7.** Effects of AAKR on apoptosis of PC12 cells induced by OGD/R. (A) Caspase-3 activity. (B) Western blot analysis for Bcl-2 and Bax. (C) Relative ratio of Bcl-2/Bax.  $n = 3$ , ### $p < .001$  vs control group, \*\*\* $p < .001$  vs OGD/R group.

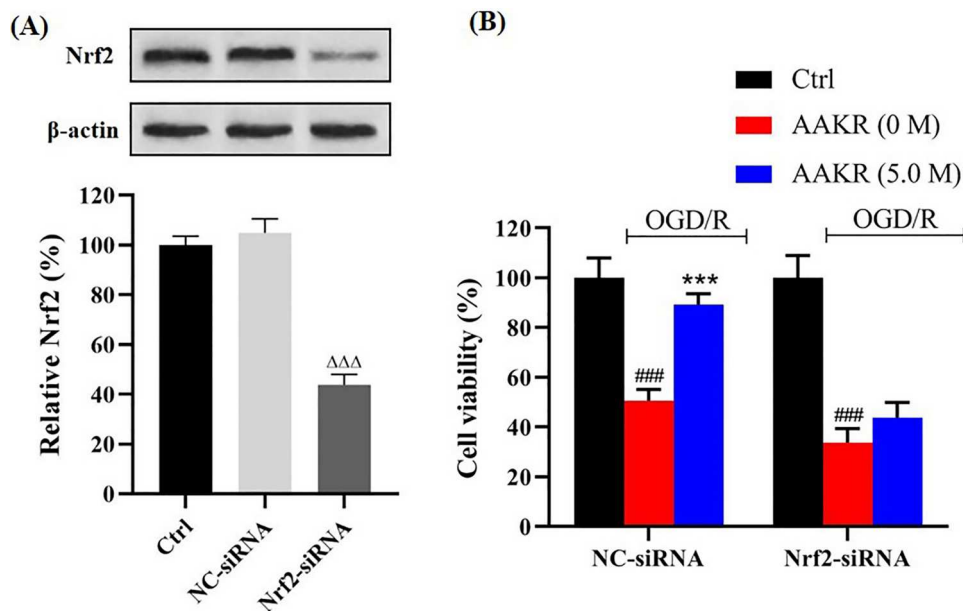


**Figure 8.** Activation of Nrf2 by AAKR was involved in the protective effects on PC12 cells against the injury induced by OGD/R. (A) Western blot together with densitometric analysis for the Nrf2 knockdown. (B) MTT assay for the PC12 cells transfected with Nrf2-siRNA or NC-siRNA exposed to OGD/R.  $n = 3$ ,  $\Delta\Delta\Delta p < .001$  vs NC-siRNA group,  $### p < .001$  vs control group,  $*** p < .001$  vs OGD/R group.

### 3.8. The protective effects of AAKR are associated with Nrf2 activation

To unravel the role of Nrf2 activation in the protective effects of AAKR, we have carried out the siRNA interference assay. As shown in Figure 8(A), the Nrf2 knockdown was attained after western blot analysis. The PC12 cells transfected with NC-siRNA were still sensitive to OGD/R and AAKR also displayed protective effects. However, in PC12 cells transfected with Nrf2-siRNA, the MTT assay showed the protective effects of AAKR were reduced sharply following the poor cell viability after exposure to OGD/R (Figure 8(B)). These results revealed activation of Nrf2 was involved in the protective effects of AAKR on PC12 cells against the injury induced by OGD/R.

### 3.9. AAKR protects mice brains against the injury induced by MCAO via activating Nrf2

To validate the neuroprotective effects of AAKR via Nrf2 activation, we have implemented the *in vivo* evaluation using MCAO mice. As a result, HE staining showed the nuclei stained as blue by hematoxylin, and the apoptotic nuclei condensed. This observation indicated that MCAO resulted in the apoptosis of neurons in mice brains, while AAKR at 50.0 mg/kg could attenuate the apoptosis. However, in the presence of Nrf2 inhibitor, ML385, the protective effects of AAKR were reduced. At the same time, from immunohistochemical assay, it was observed that AAKR decreased the expression of cleaved caspase-3 stained as brown by DAB, which was up-regulated after MCAO treatment. And ML385 could reduce the inhibitory effect of AAKR on caspase-3 (Figure 9(A)). Meanwhile, western blot together with densitometric analysis showed AAKR could increase the level of Nrf2 in the brains of MCAO mice, but ML385 reversed this effect (Figure 9(B)). In addition, the antioxidant enzymes including SOD, CAT and GPx were inhibited in MCAO mice. Whereas, AAKR could enhance the activity of these enzymes via activating

Nrf2 (Figure 9(C–E)). These findings indicated AAKR protected brains of MCAO mice against oxidative stress and apoptosis via activating Nrf2.

## 4. Discussion

In the treatment of cerebral ischemic stroke, reperfusion after cerebral ischemia largely contributes to the neural injury though it is effective to reduce the infarction size [27]. The pathogenesis of cerebral ischemia/reperfusion injury has revealed oxidative stress plays a pivotal role since it initiates the cascades of cell apoptosis [28]. At the same time, it is approved activation of Nrf2 could suppress oxidative stress and related diseases [9]. Therefore, the discovery of Nrf2 activators is a promising approach targeting cerebral ischemia/reperfusion injury, which is imperative [29]. Herein, we have evaluated the neuroprotective effects of flavonoids in *Polypodium hastatum* using PC12 cells injured by OGD/R and screened their ability of Nrf2 activation. All these flavonoids especially compound AAKR at certain concentrations could significantly improve the poor cell viability resulting from OGD/R and enhance the capability of Nrf2 binding to target genes. As a stable cytoplasmic enzyme in most cells, LDH can be released into the culture medium from cytoplasm when the cell was damaged [30]. In the current investigation, these compounds showed inhibitory effects against the release of intracellular LDH.

Oxidative stress results from the imbalance between the production and consumption of ROS, which is generated through one-electron transfers from a redox donor to molecular oxygen, and initially yields the anionic free radical superoxide. Then the superoxide can be converted to hydrogen peroxide by SOD [31]. At the same time, the hydrogen peroxide is decomposed as water under the catalysis of CAT or GPx [32]. Following oxidative stress, excessive ROS will present deleterious effects on lipids, proteins, and nucleic acids, which not only leads to the reduced activity of antioxidant enzymes but also the overproduction of MDA [33]. In addition, it is proved that Nrf2 can regulate

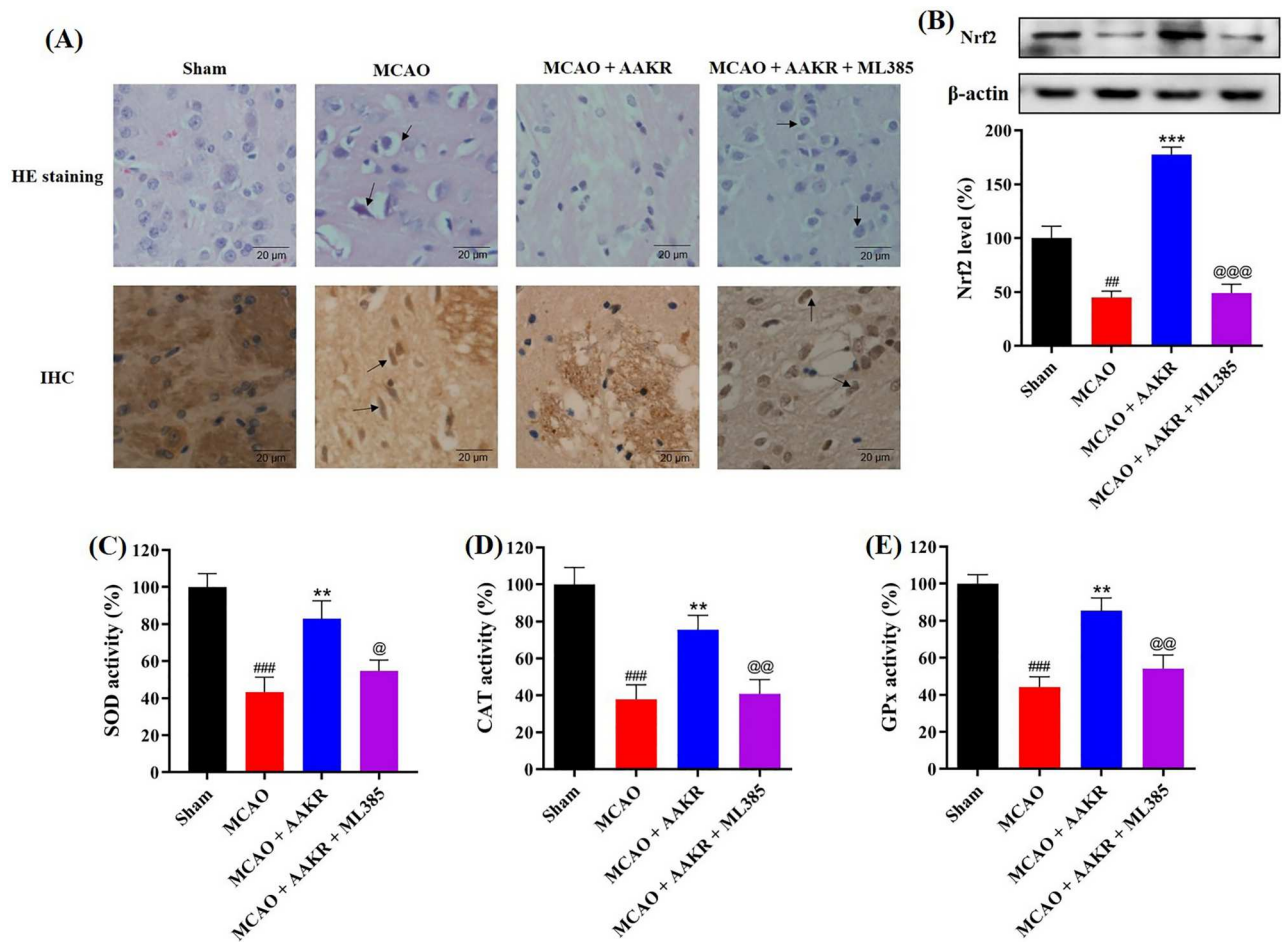


**Figure 9.** AKRR protected MCAO mice brains via activating Nrf2. (A) HE staining and immunohistochemical assay for cleaved caspase-3, and the arrows indicated morphological changes apoptotic cells and the expression cleaved caspase-3 stained as brown. (B) Western blot together with densitometric analysis for Nrf2 level. (C)–(E) SOD, CAT and GPx activity in mice brain tissues.  $n = 3$ , ### $p < .01$  and #### $p < .001$  vs sham group, \*\* $p < .01$  and \*\*\* $p < .001$  vs MCAO group, @ $p < .05$ , @@ $p < .01$  and @@@ $p < .001$  vs MCAO + AAKR group.

the transcription of genes encoding these antioxidant enzymes [34]. In our investigation, we have found AAKR suppressed oxidative stress in PC12 cells and MCAO mice.

As the major sites of ROS production, mitochondria are also the target of ROS and mediate the apoptosis induced by excessive ROS [35]. The amplified ROS signal can lead to the mitochondrial permeability transition pore opening as the response to an oxidative challenge [36]. Following that, the large conductance can result in the collapse of mitochondrial membrane potential and overloaded intracellular calcium, since the mitochondrial calcium influx is driven by mitochondrial membrane potential [37]. In addition, there is a mutual interplay between ROS and calcium and excessive ROS can recruit calcium in cytoplasm [38]. And the calcium can trigger the opening of mitochondrial permeability transition pore [39]. As the early events in apoptosis, mitochondrial dysfunction including mitochondrial permeability transition pore opening and collapse of mitochondrial membrane potential is a prominent feature in neuronal cell survival and death following injury [40]. Herein, it was observed that AAKR could improve the overload of intracellular calcium, collapse of mitochondrial membrane potential and mitochondrial permeability transition pore opening, which implied AAKR can mitigate mitochondrial dysfunction due to OGD/R.

In ischemic stroke, neurons undergoing apoptosis in penumbra are potentially salvageable and predominant in the expansion of infarction size [41]. In the pathogenesis of

ischemia/reperfusion injury, rapid overproduction of ROS overwhelms the detoxification and scavenging capacity of cellular antioxidant enzymes viz SOD, CAT, and GPx as well as non-enzymatic antioxidants such as GSH, which results in severe and immediate damage to cellular proteins, DNA and lipids [4]. In addition to the breakdown of antioxidant defense system, excessive ROS triggers mitochondria-mediated apoptosis [35]. As the source of ROS, mitochondria in particular are susceptible to ROS, which could result in mitochondrial dysfunction and recruitment of Bcl-2 family proteins for cytochrome c release [42]. Then the released cytochrome c forms the apoptosome complex to activate the caspase cascades [43]. As the key member of caspases, caspase-3 is an effector enzyme affording the morphological changes of apoptotic cells [44]. Bcl-2 and Bax are important members of Bcl-2 protein family, and the former is anti-apoptotic while the latter is pro-apoptotic [43]. Under apoptotic stimuli such as oxidative stress, Bax in cytoplasm will be recruited to mitochondrial membrane and oligomerize to cause the release of pro-apoptotic proteins in mitochondria, which then activate caspase-3 through the intrinsic apoptotic cascades [45]. However, the anti-apoptotic Bcl-2 in the mitochondrial membrane can interact with Bax to form heterodimers, which will block the initiation of apoptotic cascades. Therefore, the relative ratio of Bcl-2/Bax is the determinant to the apoptotic stimuli [46]. In our study, we have observed AAKR inactivated the active caspase-3 *in vitro* and *in vivo*, and up-regulated Bcl-2 but down-regulated Bax, which

gave the indication that AAKR could inhibit the apoptosis of neurons.

As a crucial transcription factor, Nrf2 can regulate the transcription of target genes encoding antioxidant enzymes [47]. In addition to the direct antioxidant enzymes such as SOD, CAT and GPx, the indirect antioxidant enzymes including HO-1 and NQO1 are regulated by Nrf2 and catalyze to promote the production of antioxidant products [48]. In cerebral ischemia stroke, it was also found Nrf2 could regulate these enzymes to afford antioxidant activity [49]. In the current study, it was also found that AAKR activated HO-1 and NQO1 remarkably. The siRNA interfere experiments validated that the Nrf2 activated by AAKR was involved in its neuroprotection. Michael receptors are prominent electrophiles since there are olefins conjugated to electro-withdrawing carbonyl groups in their structures. As the soft Lewis acids, they can react with the critical cysteine thiolate (soft base) groups in Keap1 to hinder the formation of Keap1-Nrf2 complex and activate Nrf2 [17]. Herein, all these flavonoids including AAKR possess the  $\alpha,\beta$ -unsaturated ketone moieties, which may be involved in their ability to activate Nrf2.

In present studies, the protective effects of AAKR against cerebral ischemia/reperfusion injury were further evaluated using MACO mice, which was closely associated with the activation of Nrf2. However, there are many factors such as blood pressure (BP) affecting the prognosis of cerebral ischemia/reperfusion injury [50]. Meanwhile, due to the limited amount of AAKR, the evaluation and mechanisms exploration were not widely performed. In the future, the profound investigations will be carried out after the isolation of enough AAKR.

## 5. Conclusion

Collectively, we have evaluated flavonoids in *Polypodium hastatum* as Nrf2 activators using PC12 cells and MCAO mice and explored their protective effects against ischemia/reperfusion injury. Of the five flavonoids, AAKR significantly protected PC12 cells and brains of MCAO mice against oxidative stress, mitochondrial dysfunction and following apoptosis. The protective effects were closely associated with the activation of Nrf2 via interacting with Keap1. These findings can give insights into the discovery of Nrf2 activators targeting cerebral ischemia/reperfusion injury.

## Ethics approval

The protocols for animal experiments were approved by the Laboratory Animal Ethics Committee of Xuzhou Medical University (No. 202205A172) and performed under the Guide for the Care and Use of Laboratory Animals (Eighth Edition).

## Acknowledgements

Huankai Yao: Conceptualization, Investigation, Methodology, Formal analysis, Writing – original draft. Ruiqing Wu: Investigation, Data curation, Methodology. Dan Du: Data curation, Formal analysis, Validation. Fengwei Ai: Data curation, Formal analysis. Feng Yang: Methodology, Formal analysis. Yan Li: Conceptualization, Funding acquisition, Project administration, Resources, Supervision, Validation, Writing – review & editing. Suhua Qi: Conceptualization, Methodology, Resources.

## Disclosure statement

No potential conflict of interest was reported by the author(s).

## Funding

This work was supported by the Jiangsu Science and Technology Development Program of Chinese Medicine [grant number MS2022141] and Xuzhou Key Research and Development Program (Social Development) [grant number KC22121].

## Data availability statement

The data used to support the findings of this study are available from the corresponding author upon reasonable request.

## ORCID

Yan Li  <http://orcid.org/0000-0001-5723-6936>

## References

- [1] Pandian JD, Gall SL, Kate MP, et al. Prevention of stroke: a global perspective. *Lancet*. 2018;392(10154):1269–1278. doi:10.1016/S0140-6736(18)31269-8
- [2] Zerna C, Thomalla G, Campbell BCV, et al. Current practice and future directions in the diagnosis and acute treatment of ischaemic stroke. *Lancet*. 2018;392(10154):1247–1256. doi:10.1016/S0140-6736(18)31874-9
- [3] Paul S, Candelario-Jalil E. Emerging neuroprotective strategies for the treatment of ischemic stroke: an overview of clinical and preclinical studies. *Exp Neurol*. 2021;335:113518, doi:10.1016/j.expneurol.2020.113518
- [4] Mehta SL, Manhas N, Raghurib R. Molecular targets in cerebral ischemia for developing novel therapeutics. *Brain Res Rev*. 2007;54(1):34–66. doi:10.1016/j.brainresrev.2006.11.003
- [5] Granger DN, Kvietys PR. Reperfusion injury and reactive oxygen species: the evolution of a concept. *Redox Bio*. 2015;6:524–551. doi:10.1016/j.redox.2015.08.020
- [6] Schmidlin CJ, Dodson MB, Madhavan L, et al. Redox regulation by NRF2 in aging and disease. *Free Radic Biol Med*. 2019;134:702–707. doi:10.1016/j.freeradbiomed.2019.01.016
- [7] Yamamoto M, Kensler TW, Motohashi H. The KEAP1-NRF2 system: a thiol-based sensor-effector apparatus for maintaining redox homeostasis. *Physiol Rev*. 2018;98(3):1169–1203. doi:10.1152/physrev.00023.2017
- [8] Shaw P, Chattopadhyay A. Nrf2-ARE signaling in cellular protection: mechanism of action and the regulatory mechanisms. *J Cell Physiol*. 2020;235(4):3119–3130. doi:10.1002/jcp.29219
- [9] Cuadrado A, Rojo AI, Wells G, et al. Therapeutic targeting of the NRF2 and KEAP1 partnership in chronic diseases. *Nat Rev Drug Dis*. 2019;18(4):295–317. doi:10.1038/s41573-018-0008-x
- [10] Mazur A, Fangman M, Ashouri R, et al. Nrf2 as a therapeutic target in ischemic stroke. *Expert Opin Ther Targets*. 2021;25(3):163–166. doi:10.1080/14728222.2021.1890716
- [11] Madden SK, Itzhaki LS. Structural and mechanistic insights into the Keap1-Nrf2 system as a route to drug discovery. *Biochim Biophys Acta Prot Proteom*. 2020;1868(7):140405, doi:10.1016/j.bbapap.2020.140405
- [12] Tong KI, Padmanabhan B, Kobayashi A, et al. Different electrostatic potentials define ETGE and DLG motifs as hinge and latch in oxidative stress response. *Mol Cell Biol*. 2007;27(21):7511–7521. doi:10.1128/MCB.00753-07
- [13] Lee S, Hu L. Nrf2 activation through the inhibition of Keap1-Nrf2 protein-protein interaction. *Med Chem Res*. 2020;29(5):846–867. doi:10.1007/s00044-020-02539-y
- [14] Jiang ZY, Lu MC, You QD. Discovery and development of Kelch-like ECH-associated protein 1 nuclear factor Erythroid 2-related factor 2 (KEAP1:NRF2) protein-protein interaction inhibitors: achievements, challenges, and future directions. *J Med Chem*. 2016;59(24):10837–10858. doi:10.1021/acs.jmedchem.6b00586
- [15] Zhang Y, Shi Z, Zhou Y, et al. Emerging substrate proteins of Kelch-like ECH associated protein 1 (Keap1) and potential challenges for the development of small-molecule inhibitors of the Keap1-nuclear factor erythroid 2-related factor 2 (Nrf2) protein-protein interaction. *J Med Chem*. 2020;63(15):7986–8002. doi:10.1021/acs.jmedchem.9b01865

- [16] Zhang DD, Chapman E. The role of natural products in revealing NRF2 function. *Nat Prod Rep.* 2020;37(6):797–826. doi:10.1039/c9np00061e
- [17] Magesh S, Chen Y, Hu L. Small molecule modulators of Keap1-Nrf2-ARE pathway as potential preventive and therapeutic agents. *Med Res Rev.* 2012;32(4):687–726. doi:10.1002/med.21257
- [18] Yao H, Duan J, Ai F, et al. Chemical constituents from a Chinese fern *Polypodium hastatum* Thunb. *Biochem Syst Ecol.* 2012;44:275–278. doi:10.1016/j.bse.2012.06.013
- [19] Yao H, Duan J, Zhang C, et al. Coumaric acid glucosides from the Chinese fern *Polypodium hastatum*. *Chem Nat Compd.* 2016;52(4):669–671. doi:10.1007/s10600-016-1735-z
- [20] Li Y, Li K, Duan J, et al. A novel heterodimer of coumaric acid glucosides from the Chinese fern *Polypodium hastatum*. *Chem Nat Compd.* 2018;54(6):1041–1043. doi:10.1007/s10600-018-2550-5
- [21] Li Y, Shi J, Sun X, et al. Theaflavic acid from black tea protects PC12 cells against ROS-mediated mitochondrial apoptosis induced by OGD/R via activating Nrf2/ARE signaling pathway. *J Nat Med.* 2020;74(1):238–246. doi:10.1007/s11418-019-01333-4
- [22] Li D, Ikeda T, Matsuoka N, et al. Cucurbitane glycosides from unripe fruits of *Lo Han Kuo* (*Siraitia grosvenori*). *Chem Pharm Bull.* 2006;54(10):1425–1428. doi:10.1248/cpb.54.1425
- [23] Siddikov DR, Bobakulov KM, Batoshov AR, et al. Phenolic compounds from the aerial part of *Geranium rotundifolium*. *Chem Nat Compd.* 2021;57(3):539–541. doi:10.1007/s10600-021-03408-9
- [24] Xu F, Matsuda H, Hata H, et al. Structures of new flavonoids and benzofuran-type stilbene and degranulation inhibitors of rat basophilic leukemia cells from the Brazilian herbal medicine *Cissampelos sicyoides*. *Chem Pharm Bull.* 2009;57(10):1089–1095. doi:10.1248/cpb.57.1089
- [25] Marzouk MM, Kawashty SA, Saleh NAM, et al. A new kaempferol trioside from *Farsetia aegyptia*. *Chem Nat Compd.* 2009;45(4):483–486. doi:10.1007/s10600-009-9402-2
- [26] Nakano K, Takatani M, Tomimatsu T, et al. Four kaempferol glycosides from leaves of *Cinnamomum sieboldii*. *Phytochemistry.* 1983;22(12):2831–2833. doi:10.1016/S0031-9422(00)97707-0
- [27] Fisher M, Savitz SI. Pharmacological brain cytoprotection in acute ischaemic stroke - renewed hope in the reperfusion era. *Nat Rev Neurol.* 2022;18(4):193–202. doi:10.1038/s41582-021-00605-6
- [28] Saito A, Maier CM, Narasimhan P, et al. Oxidative stress and neuronal death/survival signaling in cerebral ischemia. *Mol Neurobiol.* 2005;31(1-3):105–116. doi:10.1385/MN:31:1-3:105
- [29] Sadrkhanloo M, Entezari M, Oruei S, et al. Targeting Nrf2 in ischemia-reperfusion alleviation: from signaling networks to therapeutic targeting. *Life Sci.* 2022;300:120561, doi:10.1016/j.lfs.2022.120561
- [30] Mei Z, Du L, Liu X, et al. Diosmetin alleviated cerebral ischemia/reperfusion injury *in vivo* and *in vitro* by inhibiting oxidative stress via the SIRT1/Nrf2 signaling pathway. *Food Funct.* 2022;13(1):198–212. doi:10.1039/d1fo02579a
- [31] Shadel GS, Horvath TL. Mitochondrial ROS signaling in organismal homeostasis. *Cell.* 2015;163(3):560–569. doi:10.1016/j.cell.2015.10.001
- [32] Dröge W. Free radicals in the physiological control of cell function. *Physiol Rev.* 2002;82(1):47–95. doi:10.1152/physrev.00018.2001
- [33] Sies H, Berndt C, Jones DP. Oxidative stress. *Annu Rev Biochem.* 2017;86(1):715–748. doi:10.1146/annurev-biochem-061516-045037
- [34] Itoh K, Mimura J, Yamamoto M. Discovery of the negative regulator of Nrf2, Keap1: a historical overview. *Antioxid Redox Signal.* 2010;13(11):1665–1678. doi:10.1089/ars.2010.3222
- [35] Simon HU, Haj-Yehia A, Levi-Schaffer F. Role of reactive oxygen species (ROS) in apoptosis induction. *Apoptosis.* 2000;5(5):415–418. doi:10.1023/a:1009616228304
- [36] Zorov DB, Juhaszova M, Sollott SJ. Mitochondrial reactive oxygen species (ROS) and ROS-induced ROS release. *Physiol Rev.* 2014;94(3):909–950. doi:10.1152/physrev.00026.2013
- [37] Hurst S, Hoek J, Sheu SS. Mitochondrial Ca<sup>2+</sup> and regulation of the permeability transition pore. *J Bioenerg Biomembr.* 2017;49(1):27–47. doi:10.1007/s10863-016-9672-x
- [38] Görlach A, Bertram K, Hudecova S, et al. Calcium and ROS: a mutual interplay. *Redox Biol.* 2015;6:260–271. doi:10.1016/j.redox.2015.08.010
- [39] Grimm S, Brdiczka D. The permeability transition pore in cell death. *Apoptosis.* 2007;12(5):841–855. doi:10.1007/s10495-007-0747-3
- [40] Sullivan PG, Springer JE, Hall ED, et al. Mitochondrial uncoupling as a therapeutic target following neuronal injury. *J Bioenerg Biomembr.* 2004;36(4):353–356. doi:10.1023/B:JOB.0000041767.30992.19
- [41] Uzdensky AB. Apoptosis regulation in the penumbra after ischemic stroke: expression of pro- and antiapoptotic proteins. *Apoptosis.* 2019;24(9-10):687–702. doi:10.1007/s10495-019-01556-6
- [42] Circu ML, Aw TY. Reactive oxygen species, cellular redox systems, and apoptosis. *Free Radic Biol Med.* 2010;48(6):749–762. doi:10.1016/j.freeradbiomed.2009.12.022
- [43] Youle RJ, Strasser A. The BCL-2 protein family: opposing activities that mediate cell death. *Nat Rev Mol Cell Biol.* 2008;9(1):47–59. doi:10.1038/nrm2308
- [44] Porter AG, Jänicke RU. Emerging roles of caspase-3 in apoptosis. *Cell Death Differ.* 1999;6(2):99–104. doi:10.1038/sj.cdd.4400476
- [45] Siddiqui WA, Ahad A, Ahsan H. The mystery of BCL2 family: Bcl-2 proteins and apoptosis: an update. *Arch Toxicol.* 2015;89(3):289–317. doi:10.1007/s00204-014-1448-7
- [46] Ola MS, Nawaz M, Ahsan H. Role of Bcl-2 family proteins and caspases in the regulation of apoptosis. *Mol Cell Biochem.* 2011;351(1-2):41–58. doi:10.1007/s11010-010-0709-x
- [47] Tonelli C, Chio IIC, Tuveson DA. Transcriptional regulation by Nrf2. *Antioxid Redox Signal.* 2018;29(17):1727–1745. doi:10.1089/ars.2017.7342
- [48] Jung KA, Kwak MK. The Nrf2 system as a potential target for the development of indirect antioxidants. *Molecules.* 2010;15(10):7266–7291. doi:10.3390/molecules15107266
- [49] Wang L, Zhang X, Xiong X, et al. Nrf2 regulates oxidative stress and its role in cerebral ischemic stroke. *Antioxidants.* 2022;11(12):2377, doi:10.3390/antiox11122377
- [50] Gąsecki D, Kwarciany M, Kowalczyk K, et al. Blood pressure management in acute ischemic stroke. *Curr Hypertens Rep.* 2021;23(1):3, doi:10.1007/s11906-020-01120-7